A DATASET FOR THE VALIDATION OF REFLECTANCE MODELS

Andres Kuusk, Joel Kuusk, Mait Lang

Tartu Observatory, 61602 Tõravere, Estonia - (andres, joel, lang)@aai.ee

KEY WORDS: Forest reflectance, Forest structure, Optical properties

ABSTRACT:

Three mature stands at the forest test site Järvselja, Estonia are extensively measured for using as a validation dataset for heterogeneous canopy reflectance models. In order to enable the reconstruction of the 3-D architecture of these 100 x 100 m2 test plots, individual tree positions and crown dimensions were inventoried in summer 2007. In addition, leaf, needle, stem bark and branch bark visible and near-infrared (VNIR) reflectance spectra, and VNIR reflectance spectra of ground vegetation were measured. This *in situ* dataset is supported by atmospherically and radiometrically corrected Mode 3 CHRIS reflectance spectra for three view directions acquired in July 2005, and top of canopy VNIR nadir spectra from helicopter measurements in 2007 and 2008.

1. INTRODUCTION

Large-scale experiments like BOREAS and NOPEX have been carried out primarily for the detailed study of forest communities (Sellers et al., 1997; Halldin et al., 1999; Ga- mon et al., 2004) and not with the explicit purpose to gener- ate virtual validation sites suitable for the benchmarking of radiative transfer (RT) models. The fourth phase of RAdia- tion transfer Model Intercomparison (RAMI) aims at eval- uating bi-directional canopy reflectance models, proposing two different types of test environments: 1) abstract canopies, that are generated only on the basis of disc-shaped scatterers, and 2) actual canopies, that are based on inven- tories of actual forest and plantation test sites (RAMI-IV,2009). Two mature forest stands at Järvselja test site, Estonia, were suggested as target canopies at RAMI-IV (2009). Satellite and helicopter measurements of forest reflectance spectra were carried out. Top-of-canopy data are supported by detailed measurements of stand structure and optical properties of leaves, needles, stems, and ground vegetation.

2. STUDY SITE

Forest data have been collected at a test site located in Järvselja, Estonia, 27.26°E 58.30°N. The test site serves as a training base for the forestry students of the Estonian Uni- versity of Life Sciences. Previously, Järvselja has served as a test site for the VALERI project (VALERI, 2005) and the
POLDER mission (Deschamps et al., 1994).

The test site has manifold selection of stands which are reg- ularly surveyed. A forest stand is defined as a geograph- ically unified area which has a relatively uniform species composition and is managed as a single unit. The land- scape at the test site is very flat, about 50 m above sea level. There are 3561 homogeneous and regularly managed stands in the 10×10 km VALERI site. Regular forest inventory is performed every 10 years, the last complete set of measurements is from 2001. In the inventory, several forest parameters such as species composition, age, breast-height diameter, tree height, site type, etc. have been recorded for every stand.A more detailed description of the test site is provided in (Kuusk et al., 2005).

Detailed structure measurements were carried out in sum- mer 2007 in three mature stands - a 124 years old pine stand, a 49 years old birch stand, and a 59 years old spruce stand.

3. INSTRUMENTS AND

MEASUREMENTS

Satellite data were acquired with the Compact High Res- olution Imaging Spectrometer CHRIS on board of the ex- perimental satellite PROBA (Barnsley et al., 2004). Mode 3 image cubes - 18 spectral bands selected for vegetation studies - of the test site at three view angles were acquired on July 10, 2005. Images were acquired for one near nadir and two backscattering (hot-spot side) viewing geometries. Acquisition details are listed in Tab. 1.

Table 1. CHRIS acquisition details.

Scene number:	5703	5705	5707
Date	July 10, 2005		
Time, GMT	9:43:39	9:44:28	9:45:18
View nadir angle, deg	7.62	37.23	56.71
Azimuth angle[1], deg	-22.46	19.79	23.43
Ground resolution, m	17×17	21×19	28×19
Site latitude	58.30°N		
Site longitude	27.26°E		
Sun zenith angle	36.6°		
Sun azimuth angle	167.2°		
Platform altitude	562 km		
Image size, pixels	748×744		
Number of spectral bands[2]	18		

[1] Relative to the Sun azimuth.

[2] Wavelengths and bandwidths see in Tab. 3.

Date:	26 July 2006	8 August 2007	24 July 2008
Time, GMT	9:19–9:31	9:57–10:46	8:05–8:30
Sun zenith angle	40.3°–39.8°	42.3°–42.4°	45.4°–43.2°
Sun azimuth angle	158.4°–162.7°	172.6°–189.4°	133.8°–141.6°
D_{550}/Q_{550}	0.097	0.262	0.097
Observation nadir angle	0°	0°	0°
Platform altitude	100 m	80 m	80 m

D_{550}/Q_{550} - ratio of downward diffuse and total spectral fluxes at 550 nm

Hyperspectral reflectance of stands was measured with a custom-engineered visible-near-infrared (VNIR) spectrom- eter system UAVSpec. The system is based on the 256-band near-infrared (NIR) enhanced miniature spectrometer module MMS-1 by Carl Zeiss Jena GmbH, with the front- end-electronics by Tec-5 AG. The system has a wavelength range of 306-1140 nm, 15-bit digital output, and noise level of 2-3 bits. The fiber optics entrance of the spectrometer en- ables using of different fore-optics: field restrictors of var- ious field-of-view, cosine receptor, integrating sphere. The spectrometer system comprises a web camera and a GPS receiver for position tracking in airborne measurements. A PC/104-*Plus* single board computer by VersaLogic Corpo- ration running Linux operating system is responsible for system control and data acquisition. All the acquired data are stored on a CompactFlash memory card. During he- licopter measurements the UAVSpec was mounted on the chassis of a Robinson R-22 helicopter and looked vertically downward.A fore-optics of the field-of-view of 2° was used. The measurement conditions are reported in Tab. 2.

Standard equipment was used in field measurements. A FieldSpec Pro VNIR spectrometer by Analytical Spectral Devices, Inc., equipped with cosine receptor and a disk for screening direct Sun

flux was used for the measurement of spectral incoming diffuse and total flux densities during CHRIS and airborne measurements. LAI-2000 plant canopy analyzer (Li-Cor Inc.)was used for leaf area index (LAI) measurements and a Nikon Coolpix-4500 digi- tal camera equipped with fish-eye converter FC-E8 for gap fraction studies. A calibrated gray Spectralon panel was used for the calibration of spectrometers. Leaf (and shoot - conifers) reflectance was measured with the UAVSpec spectrometer using AvaSphere-50-Refl integrating sphere and AvaLight-HAL light source by Avantes BV.

Stand structure was measured with a Nikon DTM-332 To- tal station. A square plot of 100×100 m was marked in the three selected stands. Exact positions of all trees within the plot were measured. All trees were tallied. Tree height, live crown depth, and maximum crown radius were calcu- lated for all trees using regression models developed specif- ically for the study stands based on breast-hight-diameter DBH, tree height, and, in some models, also relative DBH of the tree within a 4 m radius for sample trees. Needle and leaf masses per tree were estimated with published allo- metric foliage mass models (Hoffmann and Usoltsev, 2002; Johansson, 2000; Marklund, 1988; Tamm, 2000; Wang, 2006). Specific leaf weight was used to calculate needle and leaf area (Niinemets and Kull, 1994; Pensa and Sellin, 2002), and finally also allometric leaf area index LAI_{all} of the stands.

Effective leaf area index LAI_{eff} was measured with an LAI-2000 instrument on the regular grid of 9 sample plots (L1-L9), the grid step being 30 m. Hemispherical color (RGB) images were taken at every LAI point early in the morning with low Sun and no clouds. The blue images were thresholded for estimating gap fractions. The Cajanus sighting tube was used to obtain canopy cover and crown cover estimate (Jennings et al., 1999) according to the methodology by Korhonen, et al. (2006). Canopy cover is the proportion of canopy overlying the forest floor and crown cover is the ratio of total area of crown projections to the plot area. In the birch stand effective LAI was measured and hemispherical images were taken twice - with full foliage in July and with no leaves in winter in order to estimate the share of stems and branches in forming the canopy cover.

Reflectance spectra of ground vegetation were measured with the UAVSpec spectrometer at LAI points L1-L9 in cloudless conditions. At every LAI point radiance spectra of ground vegetation were measured vertically downward from a height of about 1 m using a field restrictor of 8° and walking along a circle of 5 m radius around the LAI point. Then the field restrictor was replaced by the cosine receptor looking upward, and the measurement was repeated. Fore-optics were leveled using self-leveling mount.

Directional-hemispherical reflectance of birch and alder leaves in the birch stand, and of spruce and pine needles was measured using the UAVSpec spectrometer equipped with the integrating sphere. Reflectance of a bundle of pine and spruce needles in a shoot was measured. Reflectance spectra of stem and branch bark were measured similarly to leaf reflectance. Stem bark reflectance of some species was measured previously with a GER-2600 spectrometer (Lang et al., 2002).

4. DATA PROCESSING

4.1 UAVSpec Measurements

In stand reflectance measurements the recorded nadir radi- ance onboard the helicopter was compared to the radiance of a calibrated Spectralon panel measured in a nearby clearing at the test site just before the airborne measurements. In this way the recorded signal is converted to the directional spectral reflectance of the targets. The diurnal changes in illumination conditions were taken into account.

Reflectance spectra of ground vegetation at every LAI point L1-L9 were calculated as the ratio of mean down-looking and up-looking signals compared to that over an accurately leveled gray Spectralon panel.

4.2 CHRIS Measurements

4.2.1 Destriping of images was performed assuming that striping is caused mainly by sensor offsets. The destriping function was found for every image as the difference between column mean values and smoothed column mean values using 9-point Hamming window (Rabiner and Gold, 1975). The mean value of three destriping functions for every band (scenes 5703, 5705, and 5707) was used for all three respective spectral images.

4.2.2 Atmospheric correction of satellite images was per- formed in two stages. First, with the atmospheric RT pack- age 6S (Vermote et al., 1997) a look-up-table (LUT) was generated which links top-of-atmosphere (TOA) radiance to top-of-canopy reflectance. The latter was calculated with the multispectral homogeneous canopy reflectance model MSRM (Kuusk, 1994) varying ground vegetation parame- ters. In the calculation of TOA radiance the optical param- eters of the atmosphere are needed. An AERONET sun- photometer (Holben et al., 1998) is working at Tartu Observatory, 45 km far from the test site, and the 6S model has tools for using AERONET sun-photometer data directly. Aerosol optical thickness, size distribution and refraction index, and amount of water vapor in the atmosphere were determined from the sun-photometer measurements. Ozone data are available from NASA/GSFC Ozone Processing Team at their web-page (McPeters, 2007). Atmospheric transparency was very high both during CHRIS and heli- copter measurements, diffuse sky flux was less than 7% of total flux in red bands and 3-5% in NIR bands.

The created LUTs were approximated by a second order polynomial separately for every CHRIS band and every view direction, The approximation polynomials were used for the calculation of top-of-canopy reflectance using the TOA radiance measured by CHRIS. This procedure was ap- plied separately to every pixel in every spectral image. The second step in the atmospheric correction procedure in- volved the removal of adjacency effects by 2-D Wiener fil- tering in the Fourier space (Banham and Katsaggelos, 1997; Podilchuk, 1998). This procedure of adjacency correction cannot be applied in the case of oblique view (the scene 5707). Then the view path crosses atmosphere layers over different targets, and the prepositions of the procedure are not fulfilled.

4.2.3 CHRIS calibration revised.

The comparison of atmospherically corrected CHRIS spectra to top-of-canopy measurements reveals problems in CHRIS radiometric calibration. Reflectance spectra of several homogeneous stands in the CHRIS scene 5703 were compared to airborne measured data. Spectral bands of the UAVSpec were combined to the equivalent CHRIS bands. The footprint of the UAVSpec spectrometer's field-of-view from the height 100 m is 9.5 m^2 which is significantly less than the CHRIS pixel, however, altogether 1302 recorded UAVSpec spectra over 520 CHRIS pixels over 63 homogeneous stands were involved in the comparison which represent all dominating species at the test site. Difference in view angles was taken into account by numerical simulations of angular dependence of stand reflectance for these targets with the FRT forest reflectance model (Kuusk and Nilson, 2000). The comparison gave us correction factors for the CHRIS cali- bration coefficients (Tab. 3).

Table 3. Mode 3 spectral bands and the corresponding cor- rection factors for CHRIS calibration

coefficients.

Band	λ	Δλ	Cλ	STD
1	442.4	10.5	0.6232	0.0669
2	490.2	11.6	0.7495	0.0830
3	530.0	11.5	0.9514	0.1000
4	551.3	12.9	0.8606	0.0904
5	570.0	10.7	0.9889	0.1096
6	631.4	14.1	1.0258	0.1245
7	661.2	15.7	1.0393	0.1419
8	674.6	11.0	1.0522	0.1485
9	697.5	11.8	0.9085	0.1034
10	706.5	6.1	0.9841	0.1052
11	712.6	6.2	1.1316	0.1200
12	741.8	13.5	0.9826	0.1029
13	752.1	7.0	1.0217	0.1061
14	781.1	22.5	1.0046	0.1018
15	872.3	27.4	0.9970	0.0956
16	895.7	18.9	1.0151	0.0951
17	910.0	9.8	0.9966	0.0929
18	1019.3	43.8	0.8935	0.0844

λ - mean wavelength, nm Δλ - bandwidth, nm
Cλ - correction factor
STD - standard deviation of the correction factor

All three sets of spectral images were radiometrically rescaled using these correction factors.

5. RESULTS

5.1 Stand Structure

The structure of the birch stand is shown in Fig. 1. A sum- mary of all tree parameters is given in Tab. 4.

5.2 Reflectance Spectra

Reflectance spectra of leaves and needles are plotted in Fig. 2. Spectra of birch and alder leaves are hard to distinguish, variance of leaf reflectance exceeds differences in mean values. Reflectance spectra of needles are those of a bunch of needles in a live shoot.

Table 4. Stand descriptions.

Stand:	Birch	Pine	Spruce
Species:	*Betula pendula* & *Alnus glutinosa*	*Pinus silvestris*	*Picea abies* & *Betula pendula*
N	990	1115	1436
H	26	16	23
DBH	21	18	23
L	10	4	11
Rcr	1.8	1.5	1.8

LAI_{eff}	2.9	1.8	3.8
LAI_{all}	3.9	1.9	4.4
CrCl	1.1	0.8	1.3
CaCl	0.80	0.74	0.90

N - number of trees; H - mean tree height, m; DBH - mean breast-height-diameter, cm;
L - mean length of live crown, m;
Rcr - mean maximum radius of crown, m; LAI_{eff} - effective LAI (LAI-2000);
CrCl - crown cover; CaCl - canopy cover.

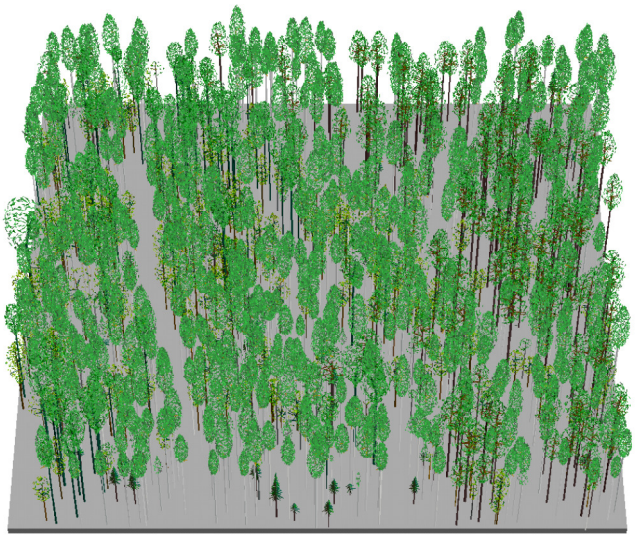

Figure 1. The birch stand. The image is created with SVS software (McGaughey, 1997).

The higher variability compared to leaves may be caused by random amount of shadows in the measured bunch.

High spatial resolution (spot diameter 1 cm) reflectance spectra of stems are very variable. Stem reflectance of dif-ferent species is very different, see Fig. 3. Brown birch branches are very dark in red, spectra of branch bark of other species are rather similar to stem bark spectra, see Fig. 4.

Reflectance of ground vegetation in the birch stand is rather typical to green vegetation. In the pine stand the sphagnum moss is yellowish green and red reflectance is about two times higher than in the birch stand. The spruce stand is dense and little light reaches the ground surface which is composed primarily of dead needles and woody material. As a consequence its reflectance spectrum is similar to that of tree stems.

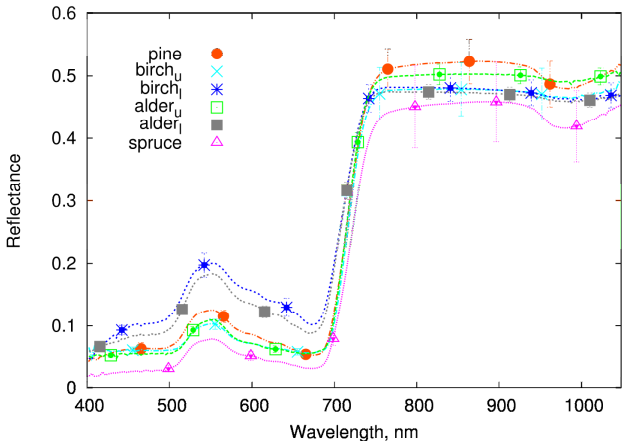

Figure 2. Reflectance spectra of leaves and conifer shoots; subscripts u and l indicate adaxial and abaxial surface of leaves, respectively.

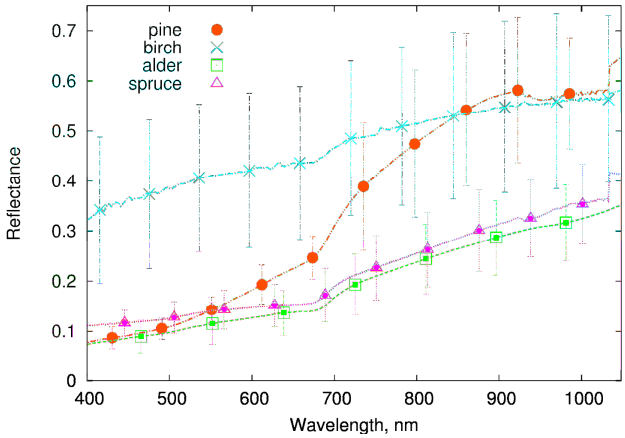

Figure 3. Reflectance spectra of stem bark.

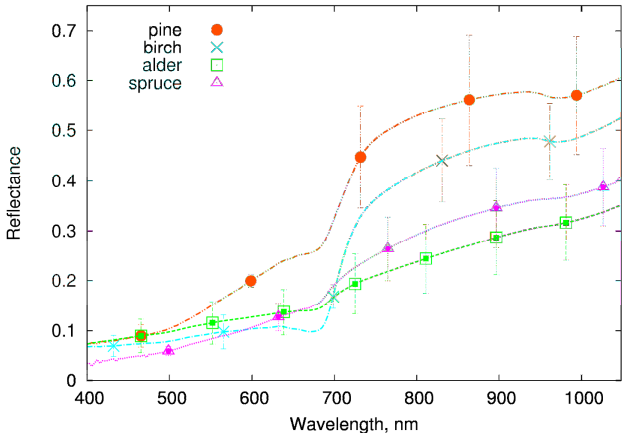

Figure 4. Reflectance spectra of branch bark.

Top of canopy directional stand reflectance both from heli- copter and satellite measurements is shown in Fig. 6-8 for the pine, birch, and spruce stands, respectively. The view zenith angle of the CHRIS scene 5705 is almost equal to the Sun zenith angle, however the difference in azimuths is about 20°, thus the view directions of scenes 5705 and 5707

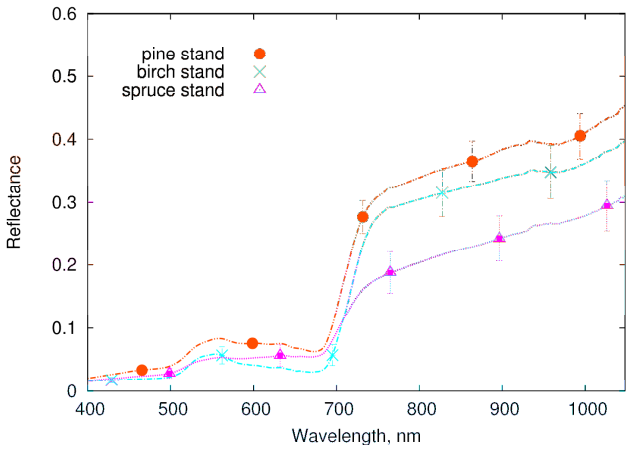

Figure 5. Reflectance spectra of understorey vegetation.

are at almost equal angular distance from the hot spot, see Tab. 1. Nadir red and blue reflectance of birch and spruce stands is extremely low - about 1.5%. The red reflectance of the pine stand is significantly higher. In the NIR the nadir reflectance of spruce and pine stands is rather equal while the deciduous birch stand is the brightest.

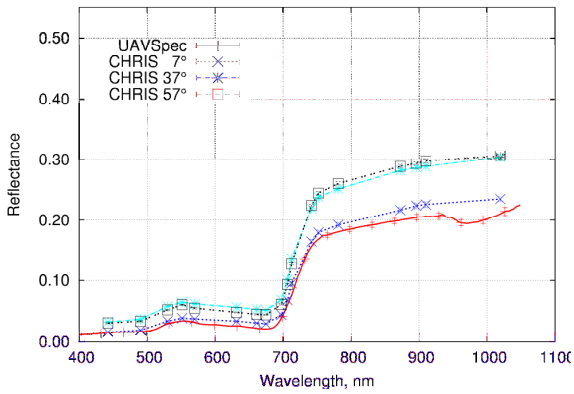

Figure 6. Reflectance spectra of the pine stand.

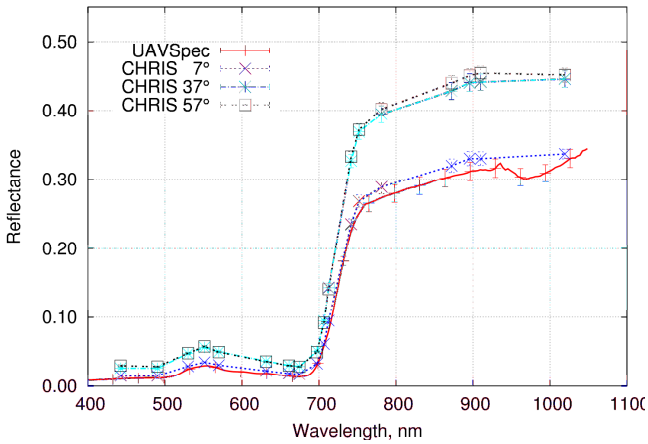

Figure 7. Reflectance spectra of the birch stand.

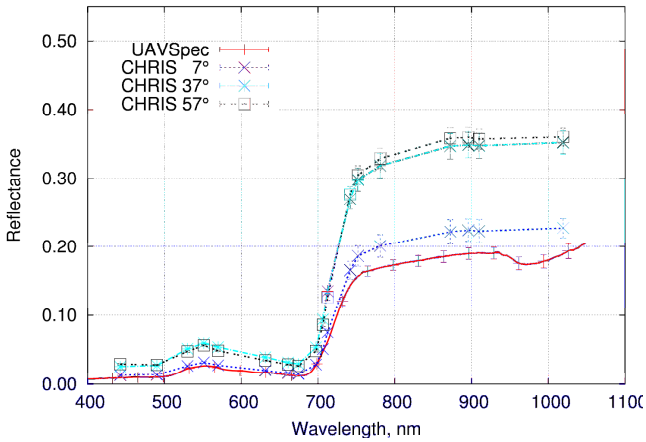

Figure 8. Reflectance spectra of the spruce stand.

6. CONCLUSIONS

The compiled dataset describes the structural and spectral properties of individual trees as well as the overall area of three hemiboreal forest stands located at the Järvselja test site in Estonia. Among others, this data set includes:

- tree positions, stem and crown dimensions, foliage mass and LAI estimates;
- reflectance spectra of leaves, needle bunches, stem and branch bark, ground vegetation, and top of canopy nadir reflectance;
- atmospherically corrected Mode 3 CHRIS directional reflectance spectra for three view directions.

All details of measurements, instruments in use, data processing, and access to data are described in the Technical Report (Kuusk et al., 2008).

Due to its exhaustive nature the data set should allow for a faithful reconstruction of the 3D canopy architecture suitable for inclusion into the latest generation of canopy reflectance models. Any thus resulting radiative transfer simulations may furthermore be compared against the remotely sensed observations of the test stands included in the dataset.

Acknowledgments

The image data presented in this paper have been provided by the European Space Agency, using the ESA PROBA platform and the Surrey Satellite Technology Ltd CHRIS instrument. The sun-photometer data are provided by the International AERONET Federation, we thank Drs. O. Kärner and M. Sulev for their effort in establishing and maintaining the Tõravere AERONET site. The European Commission's DG Joint Research Center (Ispra, Italy) sup-ported the collection of field data. Contributions by Drs. Miina Rautiainen, Tiit Nilson, Tõnu Lükk, Alo Eenmäe, Jean-Luc Widlowski, and Matti Mõttus are greately appreciated. The study has been supported by Estonian Science Foundation, Grants no. 6100, 6812 and 6815.

References

Banham, M. R., Katsaggelos, A. K., 1997. Digital image restoration. *IEEE Signal Processing Magazine*, 14, pp. 24–41.

Barnsley, M. J., Settle, J. J., Cutter, M. A., et al., 2004. The PROBA/CHRIS mission: A low-cost smallsat for hyper- spectral multiangle observations of the earth surface and atmosphere. *IEEE Transactions on Geoscience and Re- mote Sensing*, 42(7), pp. 1512–1520.

Deschamps, P. Y., Breon, F. M., Leroy, M., et al., 1994. The POLDER mission - instrument characteristics and scientific objectives. *IEEE Transactions on Geoscience and Remote Sensing*, 32(3), pp. 598–615.

Gamon, J. A., Huemmrich, K. F., Peddle, D. R., et al., 2004. Remote sensing in BOREAS: Lessons learned. *Remote Sensing of Environment*, 89(2), pp. 139–162.

Halldin, S., Gryning, S. E., Gottschalk, L., et al., 1999. En- ergy, water and carbon exchange in a boreal forest land- scape - NOPEX experiences. *Agricultural and Forest Meteorology*, 98-99(Special Issue SI), pp. 5–29.

Hoffmann, C. W., Usoltsev, V. A., 2002. Tree-crown biomass estimation in the forest species of the Ural and of Kazakhstan. *Forest Ecology and Management*, 158, pp. 59–69.

Holben, B. N., Eck, T. F., Slutsker, I., et al., 1998. AERONET - A federated instrument network and data archive for aerosol characterization. *Remote Sensing of Environment*, 66(1), pp. 1–16.

Jennings, S. B., Brown, N. D., Sheil, D., 1999. Assessing forest canopies and understorey illumination: canopy closure, canopy cover and other measures. *Forestry,* 72(1), pp. 59–74.

Johansson, T., 2000. Biomass equations for determining fractions of common and gray alders growing on abandoned farmland and some practical implications. *Biomass and Bioenergy*, 18, pp. 147–159.

Korhonen, L., Korhonen, T. K., Rautiainen, M., Stenberg,
P., 2006. Estimation of forest canopy cover: a comparison of field measurement techniques. *Silva Fennica,*
40(4), pp. 577–588.

Kuusk A., 1994. A multispectral canopy reflectance model. *Remote Sensing of Environment*, 50, pp. 75–82.

Kuusk, A., Lang, M., Kuusk, J., et al., 2008. *Database of Optical and Structural Data for the Val- idation of Radiative Transfer Models.* Technical Report. Tartu Observatory, 52 pp. Available on-line http://www.aai.ee/bgf/jarvseljadb/jarvseljadb.pdf.

Kuusk, A., Lang, M., Nilson, T., 2005. Forest test site at Järvselja, Estonia. *ESA Publication SP-593*, 7 pp.

Kuusk, A., Nilson, T., 2000. A directional multispectral forest reflectance model. *Remote Sensing of Environment*, 72, pp. 244–252.

Lang, M., Kuusk, A., Nilson, T., et al., 2002. Reflectance spectra of ground vegetation in sub-boreal forests. Web page http://www.aai.ee/bgf/ger2600/.

Marklund, L. G., 1988. *Biomass functions for pine, spruce and birch in Sweden.* Technical Report 45, Swedish Uni- versity of Agricultural Sciences, Umeå 73 pp.

McGaughey, R. J., 1997. Visualizing forest stand dynamics by using the stand visualization system. In: *Proceedings ACSM/ASPRS Annual convention and Exposition Seattle, WA. Betsheda*, Vol. 4, pp. 248–257.

McPeters, R., 2007. Total Ozone Mapping Spectrometer. Web-page http://jwocky.gsfc.nasa.gov/.

Niinemets, Ü., Kull, K., 1994. Leaf weight per area and leaf size of 85 Estonian woody species in relation to shade tolerance and light availability. *Forest Ecology and Management*, 70, pp. 1–10.

Pensa, M., Sellin, A., 2002. Needle longevity of Scots pine in relation to foliar nitrogen content, specific leaf area, and shoot growth in different forest types. *Cana- dian Journal of Forest Research*, 32, pp. 1225–1231.

Podilchuk, C., 1998. Signal recovery from partial informa- tion. In: Madisetti, V.K. and Williams, D.B., Eds., *The Digital SignalProcessing Handbook*, CRC Press LLC, Boca Raton, pp. 25-1 - 25-21.

Rabiner, L. R., Gold, B., 1975. *Theory and Application of Digital Signal Processing.* Prentice-Hall, Engelwood Cliffs.

RAMI-IV, 2009. RAdiation transfer Model Intercompari- son, Web page http://rami-benchmark.jrc.ec.europa.eu/.

Sellers, P. J., Hall, F. G., Kelly, R. D., et al., 1997. BOREAS in 1997: Experiment overview, scientific re- sults, and future directions. *Journal of Geophysical Re- search–Atmospheres*, 102(D24), pp. 28731–28769.

Tamm, Ü., 2000. *Aspen in Estonia.* Eesti Loodusfoto, Tartu, pp. 125–134.

VALERI, 2005. http://www.avignon.inra.fr/valeri/, accessed on March 15, 2005.

Vermote, E. F., Tanre, D., Deuze, J. L., et al., 1997. Second simulation of the satellite signal in the solar spectrum, 6S - An overview. *IEEE Transactions on Geoscience and Remote Sensing*, 35(3), pp. 675-686.

Wang, C., 2006. Biomass allometric equations for 10 co- occurring tree species in Chinese temperate forests. *For- est Ecology and Management*, 222, pp. 9–16.